Hindawi
Journal of Advanced Transportation
Volume 2023, Article ID 8684886, 11 pages
https://doi.org/10.1155/2023/8684886

Research Article

An Improved Adaptive Simulated Annealing Particle Swarm Optimization Algorithm for ARAIM Availability

Ershen Wang,[1,2] **Xiaozhu Shi**,[1,3] **Xidan Deng**,[2] **Jing Gao**,[4] **Wei Zhang**,[1,3] **Huan Wang**,[2] **and Song Xu**[2]

[1]*State Key Laboratory of Air Traffic Management System and Technology, Nanjing 210007, China*
[2]*School of Electronic and Information Engineering, Shenyang Aerospace University, Shenyang 110136, China*
[3]*The 28th Research Institute of China Electronics Technology Group Corporation, Nanjing 210007, China*
[4]*School of Electric Power, Shenyang Institute of Engineering, Shenyang 110136, China*

Correspondence should be addressed to Jing Gao; gaojing1@sie.edu.cn

Received 23 August 2022; Revised 22 October 2022; Accepted 13 April 2023; Published 30 May 2023

Academic Editor: Wen Liu

Civil aviation transportation equipment is more convenient and faster than other transportation tools and is an essential part of intelligent transportation. It is significant to study the reliability of positioning information and enhance traffic safety. Advanced receiver autonomous integrity monitoring (ARAIM) can provide vertical guidance during the different navigation stages in civil aviation fields. The traditional multiple hypothesis solution separation (MHSS) algorithm distributes the probability of hazardous misleading information (PHMI) and probability of false alarm (PFA) uniformly over all visible satellites resulting in reduced global availability of ARAIM. Aiming at this problem, we proposed an adaptive simulated annealing particle swarm optimization (ASAPSO) algorithm to redistribute integrity and continuity risks and establish a protection level optimization model. Based on the real BeiDou navigation satellite system/global positioning system (BDS/GPS) data, the experimental results show that the optimized algorithm can reduce the vertical protection level (VPL), and the ARAIM global availability of BDS/GPS is improved by 1.73%~2.73%. The optimized algorithm can improve the availability of integrity monitoring at different stages of the navigation system and provide a basis for ensuring the reliability of the positioning results.

1. Introduction

The BDS-3 satellite navigation system is operating smoothly and achieving global coverage. It is playing an irreplaceable role in the future and is widely used in road, railway, water, air transportation, and other aspects of transportation. In recent years, traffic safety has become a research hotspot. The satellite navigation system is closely related to traffic situational awareness and safety supervision of intelligent vehicle navigation [1, 2]. And satellite navigation is also widely used in the aviation field [3, 4]. The integrity monitoring algorithm provides some assurance of location information reliability. Integrity algorithm is one of the utmost priorities for safety critical GNSS (global navigation satellite system). The rapid development of multiconstellation integrated navigation systems has assumed a single constellation and a single failure untenable [5–7]. The ARAIM provides localizer precision with vertical guidance up to 200 feet altitude (LPV-200) for global aircraft landing navigation [8].

Related scholars have conducted a lot of research on ARAIM availability optimization. The Gauss Newton method is used to optimize the model, and the polynomial coefficient optimization algorithm is integrated to improve the ARAIM availability [9]. The integrity risk is allocated by the binary search method to reduce the VPL value [10]. Reduce VPL by optimizing the allocation of integrity risks [11]. Genetic algorithm is used to redistribute continuity risk and integrity risk to achieve VPL optimization [12]. PSO algorithm is used to optimize the integrity risk allocation process to reduce the protection level [13]. Through the maximum minimization method, the fminimax function is

used to reasonably allocate the risk probability to reduce the VPL [14]. These researches improved the availability of ARAIM in different ways. Working Group C defined multiple hypothesis solution separation as the baseline algorithm [15]. This work focuses on VPL computation and the global availability of ARAIM [16]. Traditional risk equalization strategy leads to the conservatism of VPL. This study reallocated PHMI and PFA by using the ASAPSO to optimize availability.

The effectiveness of the ASAPSO algorithm was analyzed and validated in terms of global VPL and the ARAIM availability based on dual constellation by optimizing VPL. The results show that the optimization method based on binary constellation diagram optimized the VPL and improved the global ARAIM availability in different air navigation stages. In Section 2, the MHSS algorithm and the ASAPSO ARAIM algorithm are described in detail. In Section 3, simulations are performed using a dual-frequency carrier-smoothed position solution based on the BDS/GPS constellation. Finally, the study is concluded in Section 4.

2. ARAIM Algorithm Analysis

ARAIM algorithm uses a dual-frequency technology to eliminate ionospheric interference and uses multiple constellations to obtain more observations to enhance the global availability of LPV-200. The ARAIM algorithm is an extension of the RAIM algorithm, which requires much higher performance than the RAIM algorithm. It is a multifrequency and multiconstellation integrated navigation RAIM algorithm. ISM parameters carry information on SIS ranging error (SISRE) and fault statistics, which reflect inherent performance parameters of the core constellation, including nominal measurement biases b_{nom}, the standard deviation of ephemeris, and clock error σ_{URA}. P_{sat} and P_{const} denote the satellite failure state probability and the constellation failure priori probability, respectively. ISM parameters are generated and verified on the ground and transmitted to users as required [17, 18].

2.1. MHSS ARAIM Architecture. The MHSS algorithm is shown below [19, 20]. Based on the MHSS traditional ARAIM algorithm, it can be expressed as follows:

$$y = Hx + \varepsilon, \tag{1}$$

where H represents the observation matrix, y represents the pseudo-range observed from the navigation message and the pseudo-range residual vector calculated using the satellite position and the receiver clock error. x is the position correction parameters of the user receiver in the three-dimensional space and the receiver clock bias. ε can obey a Gaussian distribution with a mean value of zero and a variance of σ_0^2.

$$\begin{aligned} \widehat{x}_0 &= \left(H^T W^{(0)} H\right)^{-1} H W^{(0)} y = S_0 y, \\ S_0 &= \left(H^T W^{(0)} H\right)^{-1} H W^{(0)}, \\ W &= \begin{bmatrix} \dfrac{1}{\sigma_{\text{all},1}^2} & 0 & 0 & 0 \\ 0 & \dfrac{1}{\sigma_{\text{all},2}^2} & 0 & 0 \\ \vdots & \vdots & \vdots & \vdots \\ 0 & 0 & 0 & \dfrac{1}{\sigma_{\text{all,n}}^2} \end{bmatrix}, \end{aligned} \tag{2}$$

where W represents the weight matrix and $\sigma_{\text{all},i}$ represents the standard noise error of the $i-th$ satellite. The solution separation test is as follows:

$$\begin{aligned} \Delta x_i &= \left|\widehat{x}_i - \widehat{x}_0\right|, \\ &\begin{cases} \widehat{x}_0 = \left(H^T W H\right)^{-1} H^T W_i y = S_i y, \\ \widehat{x}_i = \left(H^T W H\right)^{-1} H^T W y = S_0 y, \end{cases} \end{aligned} \tag{3}$$

where $\widehat{x}_i$ represents the $i-th$ subset and $\widehat{x}_0$ represents the subset with no fault. Furthermore, the detection threshold of the vertical position corresponding to the fault subset is as follows:

$$D_i = K_{fa,i} \times \sigma_{dv,i} + \sum_{i=1}^{N_{\text{sat}}} \left|\Delta S_i(3,i)\right| \times b_{\text{cont},i}. \tag{4}$$

The ARAIM VPL calculation can be expressed as follows:

$$\begin{cases} \text{VPL}_0 = K_{md,0} \times \sigma_{v,0} + \sum_{i=1}^{N_{\text{sat}}} \left|S_0(3,i)\right| \times b_{\text{nom},i}, \\ \text{VPL}_i = D_i + K_{md,i} \times \sigma_{v,i} + \sum_{i=1}^{N_{\text{sat}}} \left|S_i(3,i)\right| \times b_{\text{nom},i}, \\ \text{VPL} = \max\left(\text{VPL}_0, \text{VPL}_i\right), \end{cases} \tag{5}$$

where VPL_i represents VPL corresponding to the fault subset. $i = 0$ denotes VPL corresponding to the fault-free subset. S_0 represents the fault subset's weighted least squares projection matrix, S_i denotes the $i - th$ fault subset, and b_{nom} represents the maximum standard deviation of the $i - th$ satellite used to evaluate the integrity; it can be expressed as follows:

$$\Delta S_i = S_i - S_0, \tag{6}$$

where $\sigma_{v,0}, \sigma_{v,i}$, and $\sigma_{dv,i}$ can be expressed as follows:

$$\begin{aligned} \sigma_{v,0} &= \sqrt{\left(\mathrm{HWH}^T\right)^{-1}_{3,3}}, \\ \sigma_{v,i} &= \sqrt{\left(H^T M_k W H\right)^{-1}_{3,3}}, \\ \sigma_{dv,i} &= \sqrt{\left(\Delta S_i W^{-1} \Delta S_i^T\right)_{3,3}}. \end{aligned} \tag{7}$$

The traditional ARAIM algorithm equally allocates the continuity and integrity risk probability to all visible satellites. The integrity constraint coefficient $K_{md,i}$ and $K_{fa,i}$ are determined by PHMI and PFA expressed as follows:

$$\begin{aligned} K_{fa,i} &= -Q^{-1}\left(\frac{\mathrm{PFA}}{N}\right), \\ K_{md,0} &= -Q^{-1}\left(\frac{\mathrm{PHMI}}{2(N+1)}\right), \\ K_{md,i} &= -Q^{-1}\left(\frac{\mathrm{PHMI}}{P_{\mathrm{sat},i}(N+1)}\right), \end{aligned} \tag{8}$$

where Q is the right hand side cumulative distribution function of a zero mean unit Gaussian. N is the number of fault subsets; traditional allocation of PHMI and PFA will lead to conservative protection levels. Therefore, the PHMI and PFA are allocated by the ASAPSO algorithm, and this allocation strategy will be discussed.

2.2. VPL Calculation of MHSS ARAIM Algorithm Optimized Based on ASAPSO. The PSO algorithm easily falls into local convergence, which leads to slowing down the overall convergence speed [21, 22]. Therefore, the simulated annealing algorithm is combined with the PSO algorithm. The algorithm is divided into two stages: the standard PSO algorithm is used for optimization in the early stage and the simulated annealing algorithm is used later to optimize and search the parameters in the PSO algorithm [23, 24].

This study proposed an optimization strategy based on the ASAPSO algorithm to solve the problem that the average distribution strategy is not optimal. The VPL is optimized by introducing an adaptive weight function. The proposed optimization algorithm can obviously reduce the vertical protection level and improve the ARAIM availability.

Step 1. Calculation of the velocity and position of particles.

$$v_m(it+1) = w v_m(it) + c_1 r_1 \left(p\mathrm{best}_m - x_m(it)\right) + c_2 r_2 \left(g\mathrm{best}_m - x_m(it)\right), \tag{9}$$

$$x_m(it+1) = x_m(it) + v_m(it+1), \tag{10}$$

where it represents the current particles number of iterations, w represents the inertia weight, c_1 and c_2 represent the acceleration constants, which are used to adjust the velocity of motion in the $p$best and $g$best directions, respectively. r_1 and r_2 are the random number between 0 and 1. x_m represents the particle's position. v_m represents the moving speed of the particle m [25, 26].

Step 2. Selection of adaptive inertia weight.

The method of adaptive inertia weight was introduced to balance the global and local search ability of the PSO and improve the algorithm's performance. The formula is as follows:

$$\omega = \begin{Bmatrix} \omega_{\min} - \dfrac{(\omega_{\max} - \omega_{\min})(f - f_{\min})}{f_{\mathrm{avg}} - f_{\min}}, f \le f_{\mathrm{avg}} \\ \\ \omega_{\max}, f > f_{\mathrm{avg}} \end{Bmatrix}, \tag{11}$$

where $\omega_{\max}$ and $\omega_{\min}$ represent the maximum and minimum values of the inertia weight w, respectively. f is the fitness value of the particles. f_{avg} and $f_{\min}$ are the average and minimum fitness values of the particles in the population, respectively [27].

If the target value region of each particle is consistent and the region is locally optimal, the inertia weight will increase. If the target value of each particle is dispersed, the inertia weight will decrease.

Step 3. Metropolis criterion updating strategy combined with the simulated annealing algorithm.

We proposed an update strategy based on the Metropolis criterion to solve the particle position update problem. First, calculate the particle's next possible position according to the updating equation (9). Then, judge whether it can be accepted as the particle's next position according to the Metropolis criterion. Finally, the steps are as follows:

$$\begin{cases} \mathrm{fit}_{i+1}(t) \le \mathrm{fit}_i(t), \\ r\mathrm{and} \le \exp\left(\dfrac{-\mathrm{fit}_{i+1}(t) - \mathrm{fit}_i(t)}{T}\right), \end{cases} \tag{12}$$

where fit_{i+1} is the fitness value for the next position of the particle. The Metropolis criterion is introduced so that the particle does not accept the different solution with full probability, but accepts probability with $\exp(-\mathrm{fit}_{i+1}(t) - \mathrm{fit}_i(t)/T) > r\mathrm{and}$. The Metropolis criterion's update strategy avoids particle degradation in some extent.

Step 4. Particle fitness function selection.

According to the MHSS algorithms, the probability average allocation method of PHMI and PFA is adopted, and the VPL calculation method can be expressed as follows:

$$\mathrm{VPL}_i = -Q^{-1}\left(\frac{\mathrm{PFA}}{N}\right) \times \sigma_{dv,i} + \left(-Q^{-1}\left(\frac{\mathrm{PHMI}}{P_{\mathrm{sat}}(N+1)}\right)\right) \times \sigma_{v,i} + \sum_{i=1}^{N_{\mathrm{sat}}} \left|S_i(3,i)\right| \times b_{\mathrm{nom},i} + \sum_{i=1}^{N_{\mathrm{sat}}} \left|\Delta S_k(3,i)\right| \times b_{\mathrm{cont},i}. \tag{13}$$

According to equation (13), VPL is taken as the optimization objective. The schemes assigned to each fault subset by PHMI and PFA are as follows:

$$\begin{aligned} &\mathrm{minmax}\left(\mathrm{VPL}_k\left(\mathrm{PHMI}_k, Pfa_k\right)\right), \mathrm{s\cdot t\cdot} \begin{cases} \sum_{k=1}^{N_{\mathrm{set}}} P_{\mathrm{HMI},k} \le \mathrm{PHMI}, \\ \sum_{k=1}^{N_{\mathrm{set}}} P_{fa,k} \le \mathrm{Pfa}, \end{cases} \\ &\mathrm{VPL} = \mathrm{min}\mathrm{VPL}_i\,(i = 0, \ldots, N), \end{aligned} \tag{14}$$

where the VPL corresponding to each fault subset is expressed as follows:

$$\mathrm{VPL}_i = -Q^{-1}\left(\frac{\mathrm{PFA}}{N}\right) \times \sigma_{dv,i} + \left(-Q^{-1}\left(\frac{\mathrm{PHMI}}{P_{\mathrm{sat}}(N+1)}\right)\right) \times \sigma_{v,i} + \sum_{i=1}^{N_{\mathrm{sat}}} \left|S_i(3,i)\right| \times b_{\mathrm{nom},i} + \sum_{i=1}^{N_{\mathrm{sat}}} \left|\Delta S_k(3,i)\right| \times b_{\mathrm{cont},i}. \tag{15}$$

Therefore, the weighted sum of VPL_i is taken as the optimization objective, expressed as follows [17]:

$$\begin{aligned} &\mathrm{min}\, G \\ &\begin{cases} G_i = \sum_{i=0}^{N_{\mathrm{set}}} y_i \times VPL_i, \\ y_i = \dfrac{\left(\sigma_{\mathrm{d}v,i} + \sigma_{v,i}\right)}{\sum_{i=0}^{N_{\mathrm{set}}} \sigma_{\mathrm{d}v,i} + \sum_{i=0}^{N_{\mathrm{set}}} \sigma_{v,i}}, \\ \mathrm{VPL}_i = K_{fa,i} \times \sigma_{dv,i} + K_{md,i} \times \sigma_{v,i} + \sum_{i=1}^{N_{\mathrm{sat}}} \left|S_i(3,i)\right| \times b_{\mathrm{nom},i} \\ + \sum_{i=1}^{N_{\mathrm{sat}}} \left|\Delta S_i(3,i)\right| \times b_{\mathrm{cont},i}, \end{cases} \end{aligned} \tag{16}$$

where G_i is optimization objective function and N_{set} represents the total number of particles.

Step 5. ASAPSO algorithm optimization VPL.

ASAPSO algorithm is introduced into the optimization process. The details are as follows:

(1) Firstly, M visible satellites were extracted and divided into M groups. Then, the PHMI was set to 0~PHMI and the PFA is set to 0~PFA. Finally, they were randomly divided into M groups and coded to form the initial population n.

$$n = \begin{bmatrix} Pfa_{m0}, Pfa_{m1}, Pfa_{m2}, ..., Pfa_{mN_{\text{set}}} \\ \text{PHMI}_{m0}, \text{PHMI}_{m1}, \text{PHMI}_{m2}..., \text{PHMI}_{mN_{\text{set}}} \end{bmatrix}. \tag{17}$$

where $m = 1,2, \ldots, n$, and n is the number of populations.

(2) Initialize the algorithm parameters.

(a) Initialize the position of particles in the population

(b) Set the initial temperature, where $T_0 = (-f_g)/(\ln 0.2)$ represents the initial temperature

(c) Initialize each parameter

The acceleration coefficient $c_1 = c_2 = 0.2$, the population particle size is set to $M = 50$, the maximum iteration times are set to 50, the maximum particle moving to speed is $v_{\max} = 2$, and the minimum moving speed is $v_{\min} = -2$. Then, the PHIMI and the PFA of each particle are calculated. Then, the fitness function is calculated. The distribution method of PHMI and PFA generated in the initial population are substituted into VPL. The individual optimal PHMI and the population optimal PFA are assigned to each particle.

(3) Iterative updating: First, the inertia weight W is updated based on equation (11). Next, based on the initial iteration value, the function value of each particle target is set to the individual optimal value, and the optimal value is selected from the individual optimal value as the global optimal value. Then, the particle position and velocity are updated according to equations (9) and (10). During each iteration, the individual optimal position $p\text{best}_m$ and the global optimal position $g\text{best}$ will be updated. Calculate the probability and generate a random r. If $r < \min[1, p]$, the particle will enter a new position and iterate again.

The particle will move to a new position by accepting a different probability. Finally, the temperature is cooled by $T_{k+1} = \partial \times T_k$. T represents the temperature, the value of ∂ generally ranges from 0.5 and 0.9, and k represents the number of iterations.

(4) Judgment termination condition: Judge whether the particle reaches the maximum iterations. If this condition is met, the optimized PHMI and PFA allocation strategy will be output to the optimized VPL. Otherwise, go back to step 2 and continue iterating updates. Finally, the VPL's optimal allocation strategy is obtained.

3. Experimental Verification and Results Analysis

3.1. Optimization Simulation of Continuous Risk and Integrity Risk Allocation Method. We extracted navigation information and observation files from the IGS website to verify the algorithm's performance. The simulation started at 00:00:00 on June 6, 2020, lasted for 12 hours, and the simulation step length was 10 minutes. This study uses the BDS/GPS constellation dual-frequency carrier smoothing method for simulation, and the experimental conditions are shown in Table 1.

Figure 1(a) shows that the number of visible satellites is relatively stable between 20 and 25. Meanwhile, Figure 1(b) shows that the GDOP is between 1.3 and 2. It can be indicated that the BDS/GPS satellites have a good space distribution in general. Figure 2(a) shows that the PFA is allocated by the ASAPSO algorithm. In this algorithm, PFA is randomly assigned to different satellites as a particle, and different satellites are allocated to different PFA. The value of PFA remains between $2.7e-6$ and $3.9e-6$. Figure 2(b) shows that the value remains between $5.7e-8$ and $9.8e-8$ by the optimized ASAPSO algorithm from the risk allocation of PHMI. The ASAPSO can optimize the risk allocation strategy of PHMI and PFA. Both PHMI and PFA are less than the threshold value. The improved algorithm allocates different values for different visible satellites, which can reduce the VPL and improve the ARAIM availability. Figure3shows that the VPL value of the ASAPSO is less than that of the traditional algorithm in any epoch, and both the traditional algorithm and the optimized algorithm are less than 35 m under GPS/BDS dual-frequency dual-system combination. Therefore, under the premise of ensuring PHMI and PFA, the ASAPSO algorithm can reduce the VPL. It can also improve ARAIM availability.

3.2. Global Availability Simulation Analysis of the Traditional and Optimized Method. This experiment uses BDS/GPS almanac data to analyze global availability. BDS data were downloaded from the Test and Evaluation Center of China Satellite Navigation System Management Office and GPS data were downloaded from the https://celestrak.com website [27]. The data were collected on January 2, 2021. The data simulation time is 3 hours with the step of 5 minutes.

The approach phases of an aircraft can be roughly divided into the nonprecision approach (NPA) and vertical guidance approach phase, which includes the APV-I, APV-II, and precision approach phase CAT-I, CAT-II, and CAT-III. Operational risks in different civil aviation approach

Table 1: ISM parameters setting.

Parameters	Definition	Setting
PHMI	Total integrity budget	$9.8e-7$
P_{fa}	Continuity budget allocated to disruptions because of false alert	$4e-6$
VAL	Vertical alert limit	35 m
EMT	Effective monitoring threshold	15 m
Constellation	Navigation constellations	GPS/BDS
P_{sat}	Priori failure probability of satellites	$1e-4$
P_{const}	Priori failure probability of constellations	$1e-5$

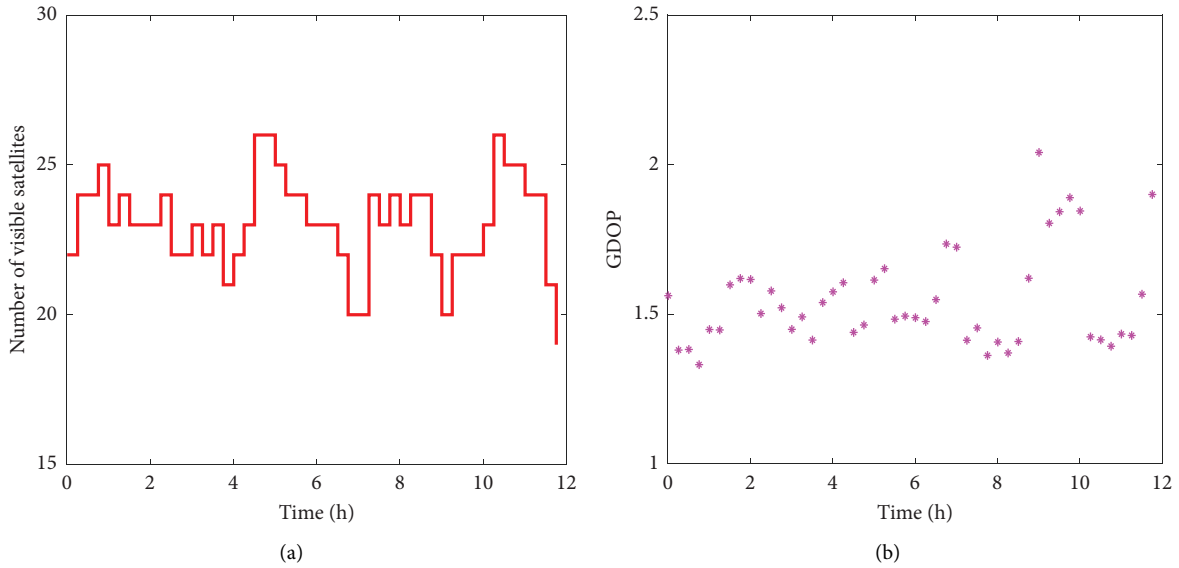

Figure 1: (a) Number of visible satellites and (b) GDOP.

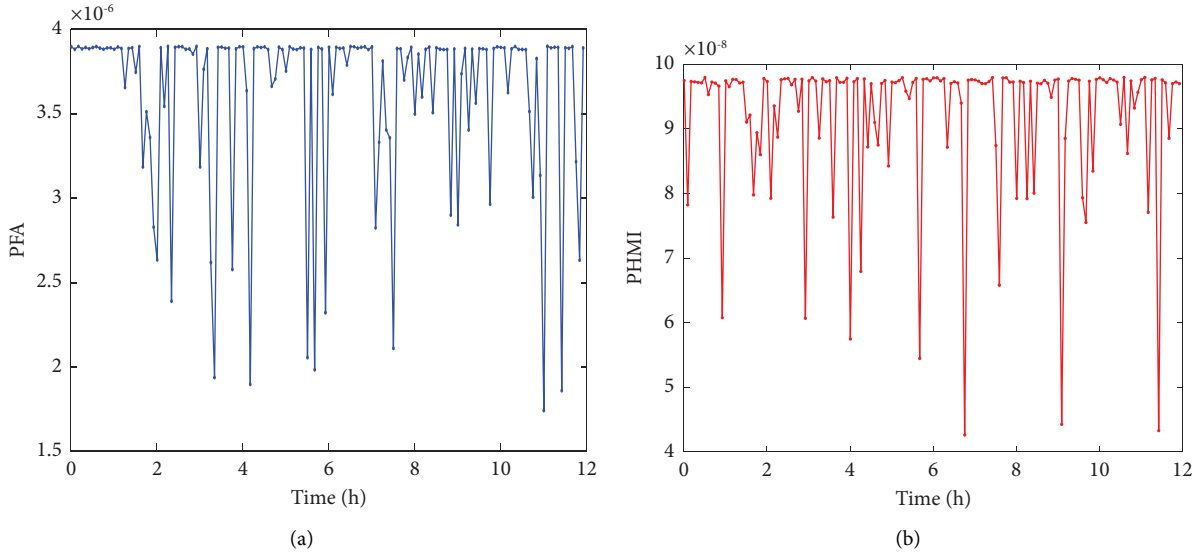

Figure 2: (a) PFA is allocated by the ASAPSO. (b) PHMI is allocated by the ASAPSO.

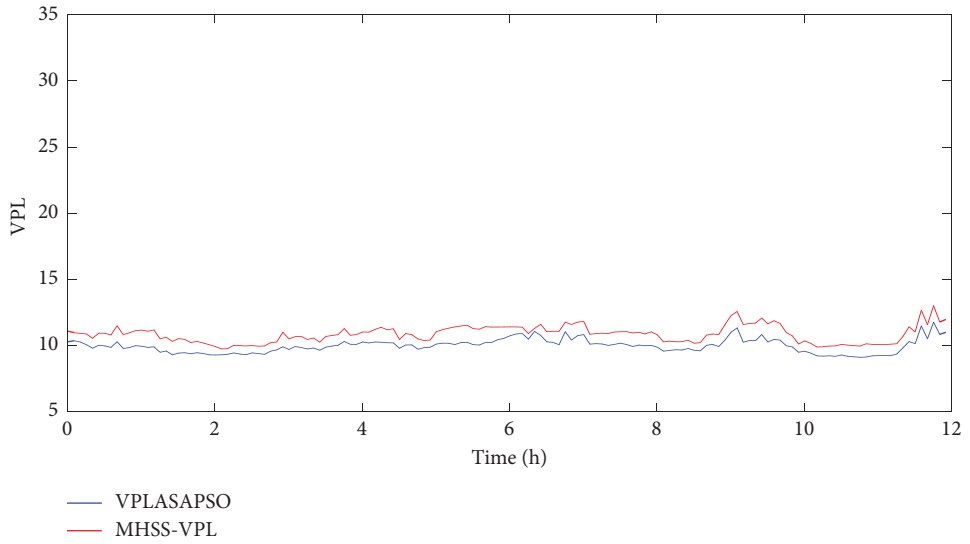

Figure 3: VPL value optimized by the MHSS algorithm and ASAPSO algorithm.

Table 2: ICAO navigation performance requirements for each approach phase.

Phase	Precision (95%)	Alarm limit	Continuity	Availability
NPA	220 m (H) N/A (V)	550 m (H) N/A (V)	1×10^{-4}/h 1×10^{-8}/h	0.99 0.99999
APV-I	16 m (H) 20 m (V)	40 m (H) 50 m (V)	8×10^{-6}/15 s	0.99 0.9999
APV-II	16 m (H) 8 m (V)	40 m (H) 20 m (V)	8×10^{-6}/15 s	0.99 0.99999
LPV-200	16 m (H) 4 m (V)	40 m (H) 35 m (V)	8×10^{-6}/15 s	0.99 0.99999
CAT-I	16 m (H) 4~6 m (V)	40 m (H) 10 m (V)	8×10^{-6}/15 s	0.99 0.99999

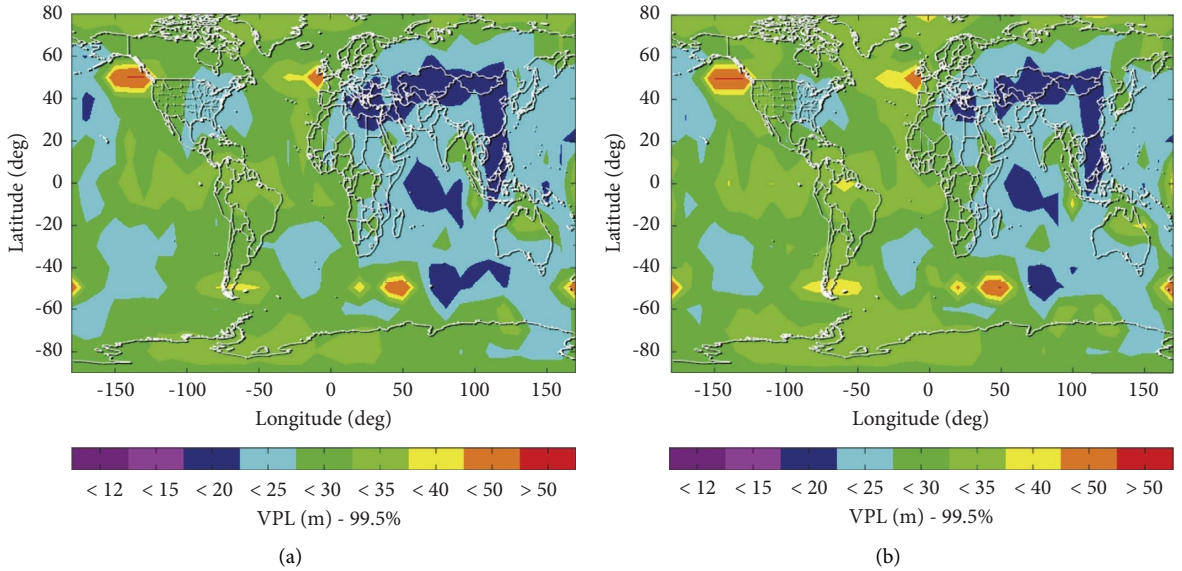

Figure 4: VPL before and after optimization. (a) VPL average = 19.7652. (b) VPL average = 20.4044.

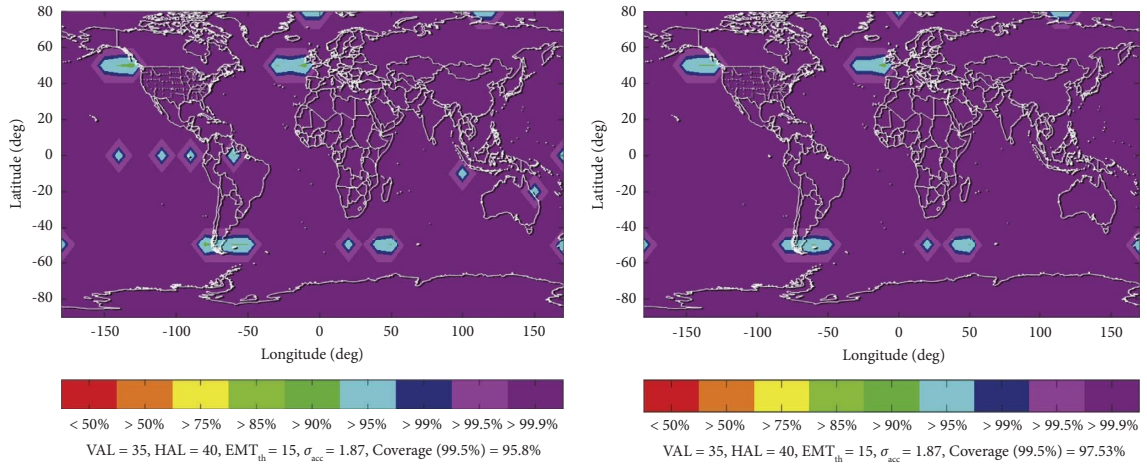

(a) (b)

Figure 5: Before and after optimization global availability of ARAIM under the LPV-200. (a) Traditional algorithm Coverage (99.5%) = 95.80%. (b) Optimized algorithm Coverage (99.5%) = 97.53%.

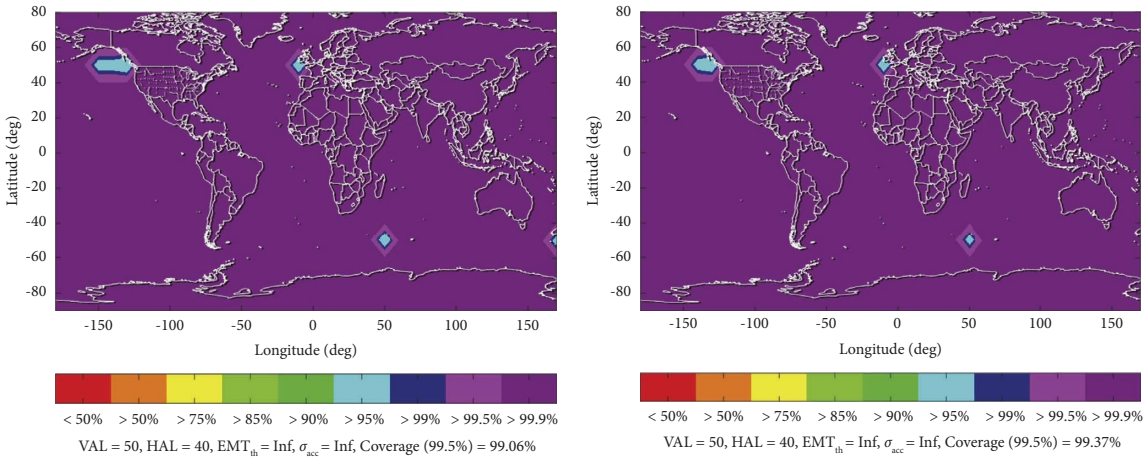

(a) (b)

Figure 6: Before and after optimization global availability of ARAIM under the LPV-250. (a) Traditional algorithm Coverage (99.5%) = 99.06%. (b) Optimized algorithm Coverage (99.5%) = 99.37%.

phases are different, so the integrity requirements of each phase are also different [28]. The ICAO (International Civil Aviation Organization) navigation performance requirements for each approach phase are shown in Table 2.

The availability of an integrity monitoring algorithm has an essential relationship with satellite geometric space distribution, which refers to the percentage of time that system functions can meet the requirements of integrity performance in a certain flight stage. Therefore, it is of great significance to study aircraft availability in different navigation stages. It is essential to analyze the availability of aircraft integrity monitoring algorithms at different navigation stages. The performance of the optimization algorithm is verified through simulation and compares whether it can meet the integrity requirements of the vertical guidance approach phase and the precision approach phase (Figures 4–8). The latitude and longitude interval is the grid spacing set by simulation, and it is selected as $10^{\circ} \times 10^{\circ}$.

Figures 4–8 show the comparison of the global VPL and availability of the traditional method (a) and the optimized method (b) under appropriate ISM parameters in different navigation stages of the BDS/GPS dual constellation. Figure 4 shows that the color of the improved algorithm gradually turns green in the range of 100°W-120° W longitude, 40°N-60°N latitude, 0°E-50°E longitude, and 40°E-60°E longitude, which plays an optimized effect. Figure 5 shows a significant improvement in the availability of the improved algorithm in the range of 25°S-20°N and 20°W to 10°E. The efficiency of the improved algorithm is obviously superior to the traditional MHSS algorithm. The MHSS algorithm is based on the spatial distribution of visible GPS satellites and uses the averaging method for risk allocation.

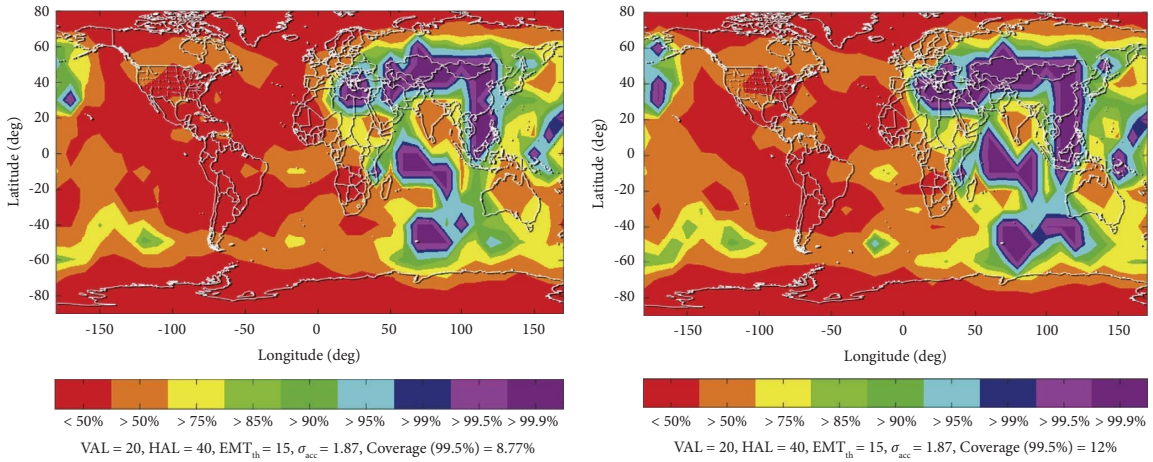

(a) (b)

Figure 7: Before and after optimization global availability of ARAIM under the APV-II. (a) Traditional algorithm Coverage (99.5%) = 8.77%. (b) Optimized algorithm Coverage (99.5%) = 12%.

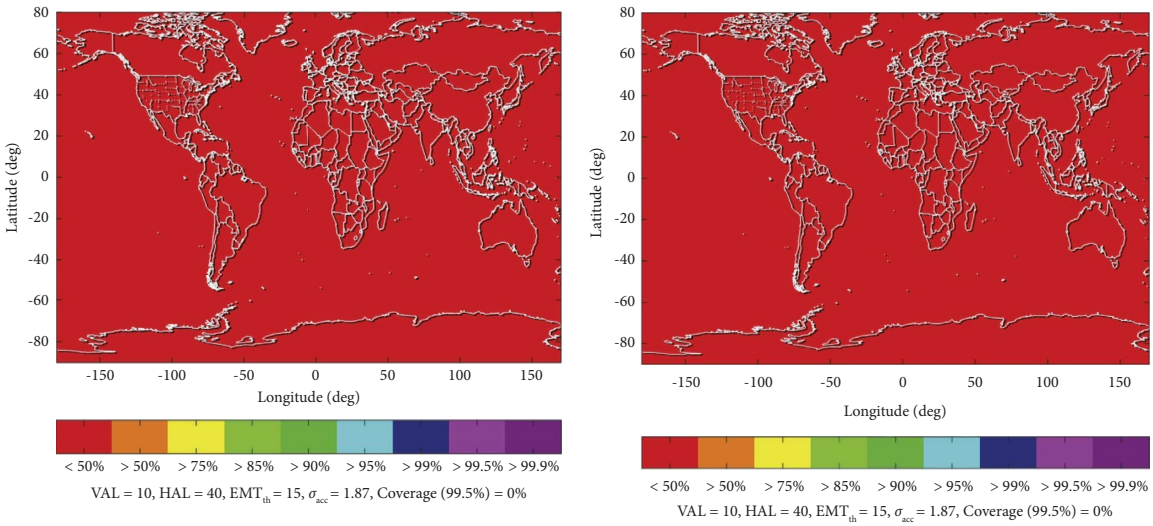

(a) (b)

Figure 8: Before and after optimization global availability of ARAIM under the CAT-I. (a) Traditional algorithm Coverage (99.5%) = 0%. (b) Optimized algorithm Coverage (99.5%) = 0%.

Table 3: Global availability ARAIM comparison between before and after optimization.

Navigation stages	Traditional algorithm (%)	Optimized algorithm (%)
LPV-200	95.8	97.53
LPV-250	99.06	99.37
APV-II	8.77	12
CAT-I	0	0

The space geometry distribution of GPS satellite is uniform, the constellation fault probability is low, and the protection level calculation under various fault assumptions is similar. For BDS/GPS integrated navigation system, BDS performance is weak, and BDS constellation distribution is uneven. Satellites of different Beidou constellations have different effects on positioning errors. Therefore, the traditional average distribution method will lead to VPL being too conservative, which will reduce the global availability of ARAIM.

Figures 5–8 show a global availability analysis of navigational integrity requirements at different navigational performance stages. Figure 5 shows that the improved algorithm is significantly improved in the range of 20°N–20°S and 40°N–60°N. And it can be found that the lower the availability before the improvement is, the more obvious the availability after the optimization algorithm is adopted. Figure 6 shows that the improved algorithm optimizes the range of 40°N–60°N and 100°W–120° W. Figure 7 shows a significant improvement in the area near the tropics. Figure 8 shows that neither algorithms can satisfy the availability of the CAT-I approach navigation stage. Table 3 shows the global availability ARAIM comparison before and after optimization in different navigation performance stages.

Table 3 shows that the global availability effect of the traditional allocation method and ASAPSO algorithm is excellent under the LPV-250 because the vertical alarm limit (VAL) of ARAIM is 50 m under the LPV-250. The VAL is much higher than the VPL. It can meet the ARAIM availability under LPV-250. However, in the LPV-200 navigation stage, the global availability of the optimized algorithm is higher, and the availability of the ARAIM is more than 90%. The ARAIM VAL is 35 m under the LPV-200. Therefore, the availability of ARAIM under the LPV-200 is significantly lower than that of the LPV-250 navigation stage in terms of global availability. The global availability of the traditional and optimized algorithm is about 8% and 12% under the APV-II navigation stage. Because the VAL required is 20 m under the APV-II. In the CAT-I stage, the VAL of ARAIM is stricter than APV-II. And the VAL is 10 m, which is far lower than the VPL. It cannot meet the integrity requirements in the CAT-I navigation stage. In addition, it can be seen that the availability of ARAIM under LPV-250 > LPV-200 > APV-II > CAT-I is under the same ISM parameter. The improved optimization algorithm has the most obvious effect on the ARAIM availability under the LPV-200 and APV-II. However, the impact of LPV-250 and CAT-I is not obvious and needs improvement.

3.3. Complexity Analysis. Theoretically, the algorithm's time complexity cannot be calculated directly, and it needs to be tested on computers. Moreover, the running time on different computers may be different, so we just analyze the time-frequency and time complexity. For the ASAPSO optimization algorithm, the population size is recorded as n, and the time-frequency, that is, the number of iterations, is recorded as $T(n)$. When n changes, $T(n)$ will also change. The time complexity of the ASAPSO is $T(n)\mathrm{O}(n^2)$. However, it does not exceed the alarm time specified by ICAO, and the global availability of the algorithm has been improved.

4. Conclusions

The ASAPSO algorithm optimized the risk allocation of PHMI and PFA and improved ARAIM availability. In different navigation stages, the degree of availability optimization of the improved algorithm is different. The availability is improved by 1.73%~2.73%. It can meet more stringent navigation phase requirements for integrity performance.

In 2020, the BDS-3 system was built successfully. And it provides global services. This study used BDS-3 actual data validated and compared the optimization and conventional algorithms. The ARAIM availability was obviously improved. With the navigation performance requirement of aviation users, the integrity of navigation performance becomes extremely important. This study presented an optimized PHMI and PFA risk allocation method. The experiment shows that the proposed algorithm can significantly improve ARAIM availability and provides more reliable services for aviation users. And the ongoing transportation revolution (especially autonomous transport systems) has significance in this work. It can provide safer and more reliable positioning information for users.

Data Availability

The data used to support the findings of this study are included within the article.

Conflicts of Interest

The authors declare that they have no conflicts of interest.

Acknowledgments

This study was supported by the National Natural Science Foundation of China (62173237), the Open Fund of State Key Laboratory of Air Traffic Management System and Technology (SKLATM202101), the Applied Basic Research Programs of Liaoning Province (2022020502-JH2/1013 and 2022JH2/101300247), the Open Fund of Key Laboratory of Civil Aviation Flights Wide Area Surveillance and Safety Control Technology of Civil Aviation University of China (202105), the Open Fund of Key Laboratory of Flight Techniques and Flight Safety, CAAC (FZ2021KF15 and FZ2021ZZ06), and the Special Funds Program of Shenyang Science and Technology (22-322-3-34).

References

[1] W. Liu, L. M. H. Liu, and J. T. Nan, "Deep learning-powered vessel trajectory prediction for improving smart traffic services in maritime internet of things," *IEEE Transactions on Network Science and Engineering*, vol. 14, pp. 290–294, 2021.

[2] D. B. Xue, L. T. Hsu, C. L. Wu, and C. Hung, "Cooperative surveillance systems and digital-technology enabler for a real-time standard terminal arrival schedule displacement," *Advanced Engineering Informatics*, vol. 50, Article ID 101402, 2021.

[3] S. I. You and S. G. Ritchie, "Tour-based truck demand modeling with entropy maximization using GPS data," *Journal of Advanced Transportation*, vol. 2019, Article ID 5021026, 11 pages, 2019.

[4] T. Y. Zhou and B. W. Lian, "A multipath processing technology based on multiparameter-combined observation in

GNSS," *Mobile Information Systems*, vol. 2021, Article ID 5574443, 11 pages, 2021.

[5] J. X. Liu, J. T. Teng, and R. Li, "Method for reducing the number of ARAIM subsets," *Journal of Beijing University of Aeronautics and Astronautics*, vol. 46, no. 8, pp. 1–11, 2020.

[6] R. Li, S. Zheng, E. Wang, J. Chen, and S. Feng, "Advances in BeiDou navigation satellite system (BDS) and satellite navigation augmentation technologies," *Satellite Navigation*, vol. 1, no. 1, pp. 1–23, 2020.

[7] E. S. Wang, W. Song, Y. Z. Zhang et al., "Evaluation of BDS/GPS multi-frequency RTK positioning performance under different baseline lengths," *Remote Sensing*, vol. 14, no. 15, p. 3561, 2022.

[8] Q. Meng, L. Y. Liu, and Q. H. Zeng, "Improved ARAIM fault modes determination scheme based on feedback structure with probability accumulation," *GPS Solutions*, vol. 23, no. 1, pp. 1–16, 2019.

[9] K. Song, S. L. Fan, J. Y. Liu, and X. Y. Wang, "Optimized RAIM algorithm based on Kalman filtering and parity vector method," *Navigation and Control*, vol. 15, no. 6, pp. 101–106, 2016.

[10] J. Blanch, T. Walter, and C. Milner, "Baseline advanced RAIM user algorithm: proposed updates," *IEEE Transactions on Aerospace and Electronic Systems*, vol. 51, pp. 229–251, 2022.

[11] S. Jing and X. Q. Zhan, "Exploration of advanced RAIM to provide LPV-200 service," *Measurement & Control Technology*, vol. 31, no. 11, pp. 75–79, 2012.

[12] X. E. Zheng, C. D. Xu, and G. C. Fan, "Multi-constellation protection level optimization method using genetic algorithm," *Journal of Beijing Institute of Technology (Social Sciences Edition)*, vol. 38, no. 10, pp. 60–64, 2018.

[13] E. S. Wang, W. S. Shu, and X. D. Deng, "Vertical protection level optimization and availability analysis for advanced RAIM," *Frontiers in Energy Research*, vol. 10, Article ID 890095, 2022.

[14] Q. Q. Han, L. Wang, and S. L. Luo, "Optimal allocation of risk probability of ARAIM algorithm," *Journal of Surveying and Mapping*, vol. 50, no. 12, pp. 1751–1761, 2021.

[15] Federal Aviation Administration (Faa), "Phase II of the GNSS evolutionary architecture study," 2010, https://www.faa.gov/about/office_org/headquarters_offices/ato/service.

[16] Y. W. Zhai, X. Q. Zhan, and J. Chang, "ARAIM with more than two constellations," in *Proceedings of the ION 2019 Pacific PNT Meeting*, pp. 925–941, Honolulu, Hawaii, April 2019.

[17] Working Group, *EU-U.S. ARAIM Technical Subgroup Milestone 3 Report*, Federal Aviation Administration, Washington, DC, USA, 2016.

[18] Working Group, *EU-U.S. ARAIM Concept of Operation*, Federal Aviation Administration, Washington, DC, USA, 2017.

[19] R. C. Eberhart and Y. H. Shi, "Particle swarm optimization: developments, applications and resources," in *Proceedings of the 2001 congress on evolutionary computation*, pp. 27–30, South Korea, May 2021.

[20] E. S. Wang, C. M. Sun, and C. Y. Wang, "A satellite selection algorithm based on adaptive simulated annealing particle swarm optimization for the BeiDou Navigation SatelliteSystem/GlobalPositioning System receiver," *International Journal of Distributed Sensor Networks*, vol. 17, no. 7, pp. 178–188, 2021.

[21] C. Chen, B. Xu, and Y. Wu, "PSOU-net: a neural network based on improved particle swarm optimization for breast ultrasound image segmentation," in *Proceedings of the 2021 2nd International Conference on Artificial Intelligence and Computer Engineering (ICAICE)*, pp. 491–498, Hangzhou, China, November 2021.

[22] Z. C. Yan and Y. S. Luo, "A particle swarm optimization algorithm based on simulated annealing," *Advanced Materials Research*, Trans Tech Publications Ltd, , vol. 989, pp. 2301–2305, 2014.

[23] Q. M. Yan, R. Q. Ma, Y. X. Ma, and J. J. Wang, "An adaptive simulated annealing particle swarm optimization algorithm," *Journal of Xi'an University of Engineering Science and Technology*, vol. 48, no. 4, pp. 120–127, 2021.

[24] J. J. Jiang, W. X. Wei, and W. L. Shao, "Research on large-scale bi-level particle swarm optimization algorithm," *IEEE Access*, vol. 9, pp. 56364–56375, 2021.

[25] E. S. Wang, C. M. Sun, and G. Tong, "Optimization method of multi-constellation GNSS vertical protection level based on particle swarm optimization algorithm," *Journal of Beijing University of Aeronautics and Astronautics*, vol. 47, no. 7, pp. 2175–2180, 2021.

[26] E. S. Wang, D. Yang, and C. Wang, "Parameter analysis and improvement of PSO satellite selection algorithm," *Journal of Beijing University of Aeronautics and Astronautics*, vol. 11, no. 5, pp. 2133–2138, 2019.

[27] L. Kuru, A. Ozturk, and E. Kuru, "Determination of voltage stability boundary values in electrical power systems by using the Chaotic Particle Swarm Optimization algorithm," *Int J Elec Power*, vol. 64, no. 15, pp. 873–879, 2015.

[28] M. Tossaint, J. Samson, and F. Toran, "The stanford – esa integrity diagram: a new tool for the user domain sbas integrity assessment," *Navigation*, vol. 54, no. 2, pp. 153–162, 2007.